JOURNAL OF CATALYSIS **168,** 374–385 (1997)
ARTICLE NO. CA971606

A Real-Time Mass Spectroscopy Study of the (Electro)chemical Factors Affecting CO_2 Reduction at Copper

P. Friebe, P. Bogdanoff, N. Alonso-Vante, and H. Tributsch

Hahn-Meitner-Institut, Abt. Solare Energetik, 14109 Berlin, Germany

Received July 26, 1996; revised November 18, 1996; accepted December 13, 1996

The electrochemical reduction of carbon dioxide at copper in a hydrogen carbonate electrolyte saturated with CO_2 was investigated using differential electrochemical mass spectroscopy and improved experimental and data processing techniques. The poisoning effects were investigated and it is shown that the deactivation of the copper cathode could be decreased by application of anodic pulses to the cathode and/or by addition of Cu^{2+} ions into the electrolyte. A soluble CO_2 reduction product of yet unknown structure with a very low vapor pressure was found in the electrolyte. The accumulation of this compound led to a remarkable decrease of the activity of copper electrodes. It is confirmed that methane and ethene are the main reduction products on the copper cathode. A new product which gave a mass signal of $m/e = 31$ was detected. The activity of methane and ethene production and the stability of the copper electrode are influenced by the nature of the alkali ion in the hydrogen carbonate electrolyte. The course of deactivation as a function of the nature of the alkali ion as well as impedance measurements give information about the mechanism of the electrochemical CO_2-reduction at copper cathodes.

INTRODUCTION

Due to the limited availability of fossil fuel resources and the fact that carbon dioxide contributes more than 50% of the greenhouse effect, research in photochemical, electrochemical, and photoelectrochemical CO_2 reduction has strongly increased in recent years (1–3).

The technology of combustion of carbon compounds is very advanced and an energy cycle based on solar-generated reduced carbon compounds may be a very convenient approach toward a sustainable energy system. The product spectrum depends on the nature of the catalyst, and it is energetically desirable to identify compounds that might reduce CO_2 to methanol, methane, or ethene. Many metals have been studied as possible candidates (2), of which copper was found to be a promising material reducing carbon dioxide mainly to methane and ethene (4, 5), though high overpotentials (< -1.5 V) are required for such a reaction.

Differential electrochemical mass spectroscopy (DEMS) has proved to be a powerful technique for the investigation of *in situ* electrochemical processes like electrocatalysis (6–8) and photoelectrocatalysis (9–11) at which the formation of volatile products is involved. The relatively short response delay of DEMS allows the observation of processes that happen within seconds. Poisoning processes which represent one major problem in electroreduction of CO_2 (8) can be followed accurately and strategies against the deactivation can be investigated effectively.

The aim of the present work was to study the electrochemical reduction of carbon dioxide on copper in a hydrogen carbonate electrolyte solution saturated with CO_2 as a function of the alkali ion nature and to investigate deactivation effects that decrease the yield of the reduction products.

EXPERIMENTAL

Electrode Preparation

Copper electrodes (surface area 1 cm^2; thickness 1500 Å) were prepared by vacuum vapor deposition of Cu (Ventron, 99.9999%) on a ethylene–tetrafluorethylene copolymere membrane (Scimat 200/40/60). The electrochemical copper deposition was performed with 5.2 μmol Cu^{2+} in 0.5 *M* H_2SO_4 at a potential of 0.0 V vs SHE prior to the measurement.

Electrochemistry

The control of the electrode potential was provided by a HEKA potentiostat, measurements with compensated internal resistance were performed with an EG&G 273A potentiostat. An electrochemical cell made of plexiglass with a standard three-electrode arrangement was used. A platinum foil electrode was used as counterelectrode and $Hg/HgSO_4$ (+650 mV/SHE) as reference. All potentials are quoted versus the SHE.

Aqueous alkali hydrogen carbonate electrolytes containing 0.5 *M* HCO_3^- were made by dissolving alkalicarbonate in deionized water and bubbling with CO_2 (Air Liquide, 99.99%) until saturation (pH 7.3).

Since the production rate of hydrocarbons is strongly dependent on the concentration of dissolved carbon dioxide

0021-9517/97 $25.00

in the electrolyte, the latter was circulated between the electrolysis cell and an external gas absorber system where carbon dioxide was bubbled through the solution to resaturate it. In addition, CO_2 was gently bubbled through the cell.

The volatile products are evaporated from the working electrode through the permeable membrane into the vacuum system of the mass spectrometer. The spectrometer unit was a PC-controlled quadrupol mass spectrometer (Balzers; QMI 420, QME 125, QMA 125 with 90° off axis SEM) which is pumped by a turbomolecular pump (TPU 60). More details are reported elsewhere (7).

The mass detection and product identification was performed via the molecules (or fragments) of the following mass/charge ratios: hydrogen, $m/e = 2$; carbon dioxide, $m/e = 44$; methane, $m/e = 15$; and ethene, $m/e = 26$.

For the impedance measurements the potentiostat was connected to a Lock-In analyzer (EG&G 2504) with an integrated frequency generator. The applied electrode potential was scanned with an ac modulation of 5 mV (rms) at a frequency of 1 kHz. In this way the conductance and capacity signals were recorded on a XYY′-recorder.

RESULTS AND DISCUSSION

Figure 1 shows the current and mass signals as a function of the applied electrode potential (not IR-compensated) for carbon dioxide reduction at a polycristalline copper cathode in CO_2-saturated 0.5 *M* $KHCO_3$ electrolyte solution. The scanning started at a potential of 0 V going up to −2.2 V at a rate of 20 mV/s.

At a potential of −0.8 V the production of hydrogen sets on, followed by the evolution of methane, ethene, and a product which gives a mass signal of $m/e = 31$, all at the same onset potential of −1.3 V. A plot of current and mass signals shows linearity only in a short range after the onset potential of the corresponding products. At higher overpotentials the evolution of mainly hydrogen bubbles purge the electrolyte and take out part of the volatile reduction products as well as CO_2 so that the ratio of detected volatile compounds to faradaic current decreases.

In order to compare the results of various measurements and to assess their reproducibility a series of factors that have influence on the detected mass signals were taken into consideration:

—potential (U);
—uncompensated resistance of the electrolyte (ohmic drop);
—the pressure inside the mass spectrometer;
—the depletion of reduction products near the membrane by purging effect of strong hydrogen evolution;
—the CO_2 reduction activity of the electrode;
—the effective area A_{eff} and the general activity of the copper cathode;
—the gas permeability of the copper-covered Tefcell membrane; and
—the detection sensitivity of a molecule or molecule fragment.

While some factors (e.g., potential, ohmic drop, A_{eff}) directly affect the production rates via the faradaic current, others influence the detection of the mass signals without affecting the electrochemistry (e.g., membrane permeability). The above-listed factors must be taken into consideration when comparing different DEMS measurements and, if necessary, must be eliminated by standardization.

The vacuum pressure of the mass spectrometer has a proportional effect on the baseline of the detected signals and was kept at a starting value of 9.0×10^{-7} mbar. Due to strong

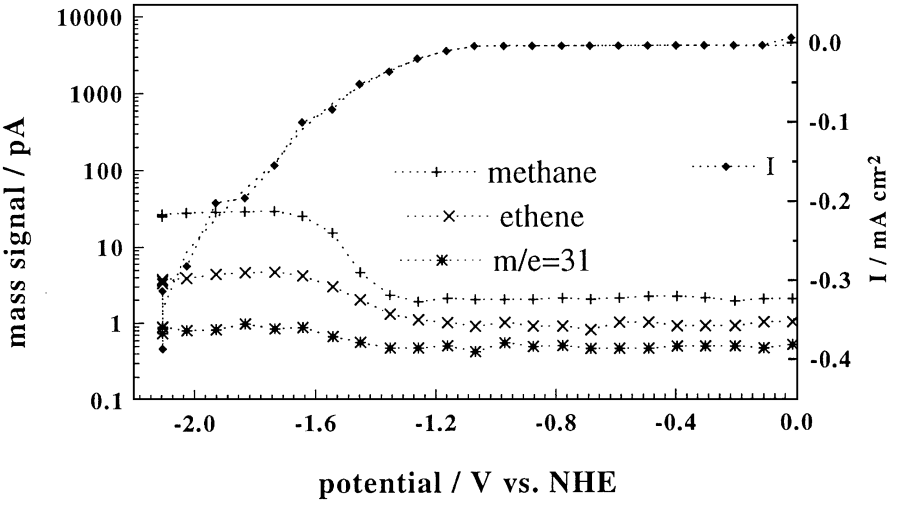

FIG. 1. Current-potential characteristic of the electrochemical reduction of carbon dioxide at a copper electrode (diamonds, right scale). Left scale: mass signals of the reduction products methane ($m/e = 15$), ethene ($m/e = 26$), and $m/e = 31$. Electrolyte: 0.5 *M* $KHCO_3$/CO_2-saturated.

hydrogen evolution at potentials <-1.2 V a purging effect decreases the detected mass signals of gaseous educts and products but should not change drastically from one measurement to another.

The detection sensitivity includes the fragmentation and ionization probability. It is a specific parameter for each compound. Thus, different mass signals must not be compared directly; i.e., equal detected mass signals of different compounds do not necessarily mean equal production rates of these compounds.

In DEMS measurements the collection efficiency CE is defined as the proportional factor between the recorded mass signal M_x of a component x and its related faradaic current I_x:

$$CE = \frac{M_x}{I_x}. \quad [1]$$

When only one compound is generated, I_x equals the cell current I. However, CE is not affected by changing from a one-component system to a multicomponent system, where several substances are generated.

The collection efficiency factor includes parameters which contain the porosity and the total collecting area A_{eff} of the working electrode as well as the detection sensitivity for the investigated molecules in the mass spectrometer.

To take the different porosities of the working electrodes into account, the hydrogen mass signal is taken as reference signal. This is done at potentials close to the onset potential of hydrogen (-1.2 V) because of the presence of a one component system, where no other reactions (CO_2 reduction) take place.

Apart from the collection efficiency of the working electrodes, their total surface area A must be taken into the standardizing calculation. The electrode surface area is proportional to the production rate and therefore to the faradaic current.

$$A = k \times I_{H_2}. \quad [2]$$

Altogether, the standardization factor N' consists of CE and A and can be written as

$$N' = CE \times A \quad [3]$$

$$= \frac{M_{H_2}}{I_{H_2}} \times k \times I_{H_2} = M_{H_2} \times k \quad [4]$$

$$N = \frac{N'}{k} = M_{H_2}. \quad [5]$$

The introduction of a dimensionless, standardized mass signal of a component x is therefore done by dividing the recorded mass signal M_x by the standardization factor N which equals the recorded mass signal of hydrogen, M_{H_2}:

$$m_x = \frac{M_x}{N}. \quad [6]$$

With these standardized mass signals it is possible to compare measurements which were carried out at copper electrodes of different porosity and surface area. Therefore, this standardization procedure was performed on measurements that included a replacement of the electrode for experiments depicted in Figs. 3 and 4a–4c.

For the standardization the mass signal of hydrogen M_{H_2} was taken at a fixed potential of -1.2 V. Division of the recorded mass signals by the corresponding hydrogen signal (at the respective potential) would lead to a lower signal-to-noise ratio of the corrected signals.

Deactivation of the Catalyst

As reported by other groups (5, 12), the copper electrode loses its activity after a short period of electrocatalysis. The majority of the reported analyses was performed by taking electrolyte samples during electroreduction, so that the deactivating process cannot be followed up very accurately. As was shown by Wasmus *et al.* (8) and will be demonstrated below, this deactivation process can be easily monitored by DEMS. To investigate the deactivation of the copper electrode, the electrolyses were performed as follows: first, the electrode potential was scanned ($v = 20$ mV/s) from 0 to -2.2 V; thereafter the latter value was held (see also potential plot in Fig. 3). The production rate of the CO_2 reduction products, shortly after the onset potential, passes a maximal value and then converges back to a value close to zero (e.g., Figs. 2 and 5). The height of the production maximum and the form of the deactivation curve depends on the conditions of electroreduction (which were kept constant), the electrolyte, and the reduction product (see Figs. 4a–4c). Poisoning occurs due to generation of an adsorbate of unknown composition on the copper cathode (8, 12) and additionally, as is shown in this work, by accumulation of a water-soluble intermediate in the electrolyte.

Addition of Cu^{2+} ions. For some measurements a constant catalytic activity was required for a long period of time. So if the catalytic activity of copper decreases because of the generation of a deactivating adsorbate, a continuous renewal of the cathode surface should lead to a constant activity for the reduction process (13). In our measurements, 4 mM $CuSO_4$ was added to the electrolyte before electroreduction (Fig. 2). During the CO_2 reduction, copper ions were reduced at the cathode and so permanently renewed the copper electrode surface. With this procedure and at a defined electrode potential the methane signal remained higher than under conventional conditions and show a slower deactivation. The course of this deactivation suggests that the main poisoning mechanism has changed. Since the concentration of Cu^{2+} ions was kept high to allow a constant renewal of the electrode surface, a poisoning adsorbate cannot be responsible for this kind of electrode deactivation. Addition of Cu^{2+} ions at the end of the measurement had no effect on the CO_2 reduction activity. So

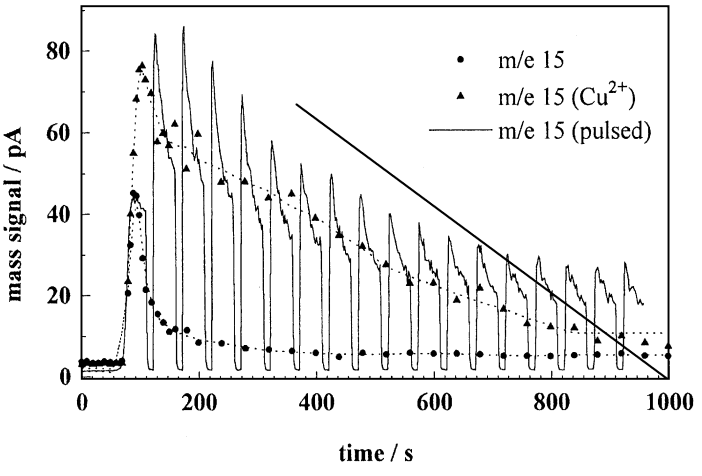

FIG. 2. Mass signals plotted versus time: CO_2 reduction with (triangles) and without (circles) addition of 4 m*M* Cu^{2+} ions to the electrolyte and with anodic pulses applied to the cathode (solid line). In the nonpulsed measurement the profile of the potential scan is the same as indicated in the legend to Fig. 3. In addition to this profile, for the anodic pulses a oxidizing period of +50 mV was applied every 50 s for 10 s.

a depletion of Cu^{2+} ions in the electrolyte is not the reason for the decrease of the production rate of methane and ethene. It is likely that a changing electrolyte composition is responsible for this poisoning effect. These assumptions will further be discussed below.

Anodic pulses. Shiratsuchi and co-workers (14) as well as Jermann and Augustynski (15) reported that the long-term activity of the copper catalyst can be sustained by a pulsed electrolysis procedure. In agreement with these observations, this effect is visualized by DEMS measurements in Fig. 2 for the methane mass signal under continuous and under pulsed anodic potentials. In this measurement, in addition to the above-explained potential profile, oxidizing potential pulses with 50 mV were applied every 50 s for 10 s.

The maximum activity of the copper electrode is reached with a slower decrease in comparison to the nonpulsed electrolysis.

The measurement under pulsed potential conditions reveals two relaxing characteristics:

First, a decay of the methane production extends over the first 700 s. The average mass signal then reaches a level which, in measurements over 3000 s remains constant. This constant level is reached within a four time longer period and whose production rate is still as high as the maximum rate of the conventional electrolysis.

Second, between each anodic pulse (where the reduction of methane immediately stops) the activity of the copper cathode decreases in a way similar to that of the long-term deactivation. This poisoning of the electrode is partially neutralized by the anodic pulse that oxidizes most of the passivating adsorbate. Thus, the local maxima just after an oxidizing pulse as well as the local minima before a pulse lead to a long-time deactivation curve similar to the curve of the nonpulsed electrolysis condition (c.f., Fig. 3).

Poisoning caused by a soluble reduction product. With the external gas-absorber system (see Experimental) the copper-coated membrane could be renewed without changing the electrolyte. The latter was stored in the gas absorber while the copper electrodes were changed. Measurements performed on a new copper cathode with used electrolyte gave much lower production rates than using

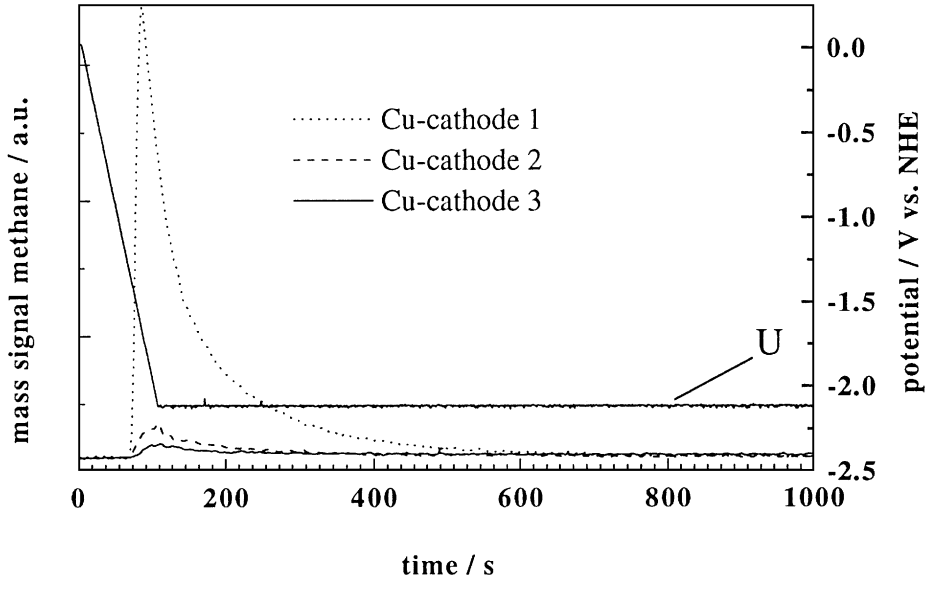

FIG. 3. Standardized mass signals of methane plotted versus time: Decrease of the reduction activity using the same electrolyte (0.5 *M* $CsHCO_3$, CO_2-saturated). The electrolyte was stored in a gas absorber when the copper cathodes were changed.

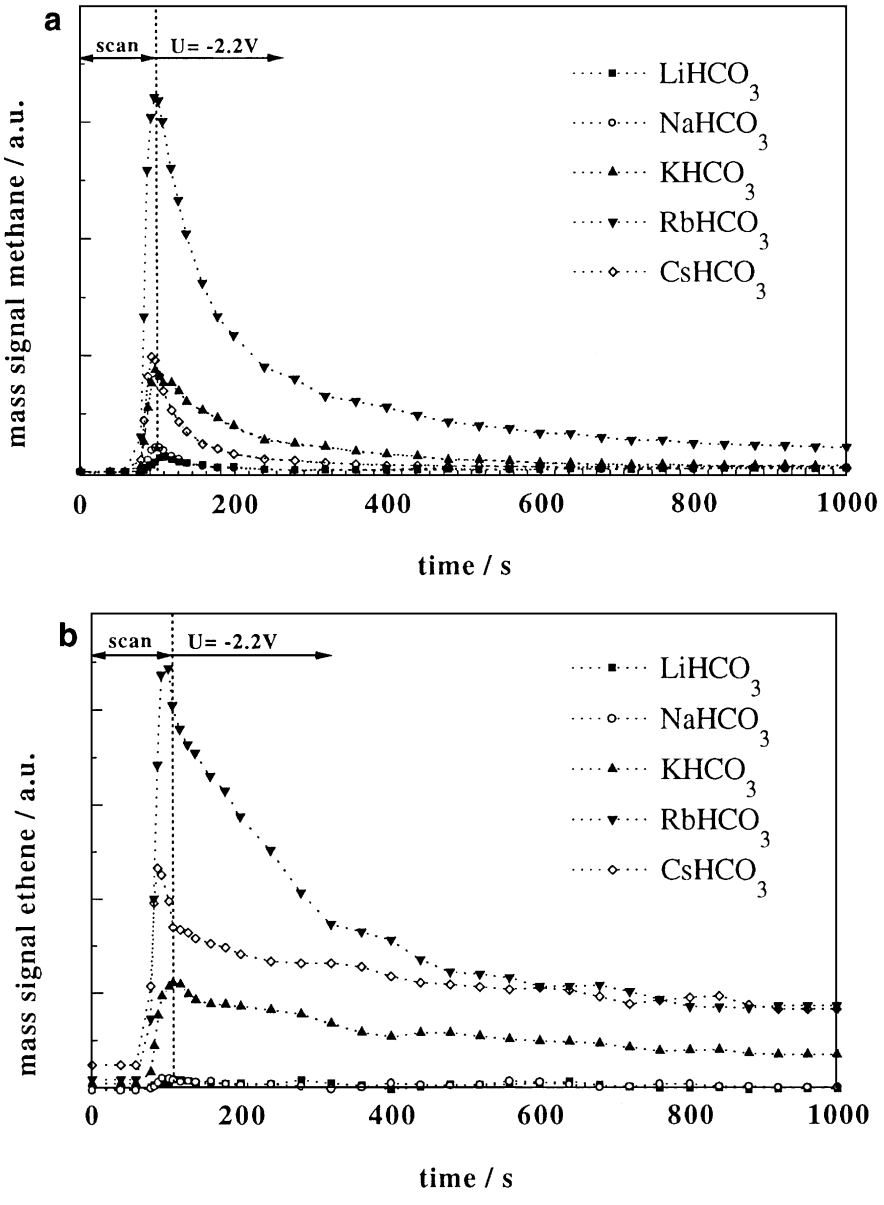

FIG. 4. Standardized mass signals plotted versus time using different electrolytes: (a) $m/e = 15$ (methane); (b) $m/e = 26$ (ethene); (c) $m/e = 31$. The profiles of the potential scan are as indicated in the legend to Fig. 3.

fresh electrolyte. Figure 3 shows three potential sweeps (performed as described above) on three copper cathodes of identical properties keeping the same electrolyte. It is clearly seen that the electroactivity of the new electrodes decreases remarkably from one sweep to the next which gives evidence that at least some poisoning intermediates are not totally fixed on the catalyst by adsorption but are soluble in aqueous solutions.

These results clearly confirm the assumptions made from the experiment in presence of Cu^{2+} ions (Fig. 2): an irreversible blocking of catalytic sites by a CO_2 reduction byproduct cannot be the only reason for a decrease in reduction activity of the copper electrode.

In previous works (12, 14, 16) it was found that under cycling conditions the copper cathode was covered with a dark film which coincided with a decrease of activity. This adsorbate was seen as graphitic carbon being a CO_2 reduction intermediate that blocks the catalytic active sites on the electrode surface. At a fixed electrode potential of -2.2 V the electrode retained its color but deactivation shows the accumulation of a poisoning adsorbate. A change of the electrolyte did not increase the activity of the cathode substantially.

In a similar experiment, the purging time for CO_2 between the first and second electroreduction performance (on different copper cathodes but with the same electrolyte)

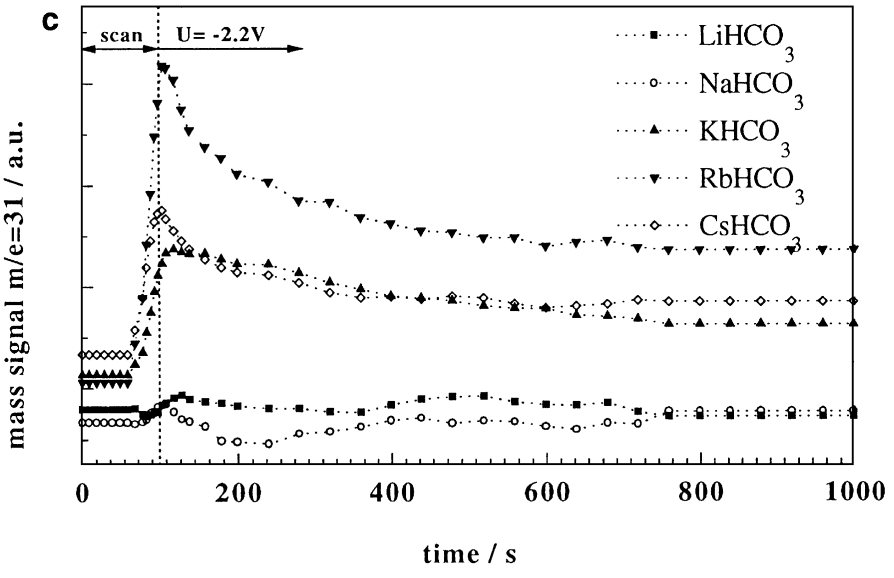

FIG. 4—*Continued*

was varied to see if the soluble poisoning product is a dissolved gas or its volatility is high enough to be driven out by purging. Prolonged CO_2 purging did not improve the activity of subsequently measured copper electrodes. Therefore, the product cannot be a dissolved gas such as carbon monoxide. Traces of a dissolved volatile but effectively poisoning compound can also be excluded; otherwise, the activity would have been zero during the following electroreduction periods using fresh electrodes (see Fig. 3).

Since the poison must come from CO_2 reduction and its volatility is negligible, the poisoning influence is probably due to one or a mixture of several higher organic compounds. Presumably traces of adsorbing substances containing several carbon atoms per molecule with an undefined structure stay in equilibrium with a desorbed species which is soluble in the electrolyte. Since, under pulsed conditions, the reduction activity reaches a constant level, it can be concluded that the adsorbed soluble poisoning species is, just as the insoluble adsorbate, oxidized to nonpoisoning compounds. As the reduction rate (pulsed electrolysis, Fig. 3) reaches a constant level, a steady state is formed where the overall rate of formation of soluble poison equals its reduction rate. This steady state is connected with a certain concentration of poison. Further investigations to obtain this state at a lower poison concentration (thus at a higher CO_2 reduction rate) as well as FTIR *in situ* measurements are underway to get more information about the mechanism of the poisoning effect.

A new reduction product? Figures 1 and 4c show the formation of a CO_2 reduction product with a m/e signal of 31 which started at the same onset potential of -1.3 V as the other products methane and ethene.

High-resolution polarographic and gas chromatographic (GC) analyses showed that no formaldehyde (which also has a $m/e = 31$ signal) down to a sensitivity of 5×10^{-6} mol/liter was present. Furthermore, high-pressure liquid chromatography (HPLC) analysis of the used electrolyte demonstrated the absence of methanol down to a sensitivity of 2×10^{-5} mol/liter.

Addition of formic acid, which is a known CO_2 reduction product at a copper electrode, did not increase the mass signal $m/e = 31$.

HPLC measurements did not show ethanol to a sensitivity of 1.4×10^{-5} mol/liter. However, few groups reported that ethanol is one CO_2 reduction product at a copper electrode (17, 18). Further investigations to clarify if $m/e = 31$ can be assigned to ethanol are still underway.

Influence of the Electrolyte Cation

As shown by other studies, coadsorption of atoms with a low work function can lead to a dramatic change of both behavior and activity of a catalyst. This effect can be observed in thermal catalysis (19–22) as well as in electrochemistry (16), although it must be assumed that the difference of reaction conditions between thermal and electrochemical catalysis leads to different reaction courses and mechanisms and thus to different effects of catalyst promotion. The influence of the alkali cation nature on the production of methane, ethene, and $m/e = 31$ is shown in Figs. 4a–4c, respectively. These mass signals were recorded keeping the electrode potential at -2.2 V after having scanned the electrode potential at a rate of 20 mV/s from 0 V (compensating the IR drop). Thereafter, they were corrected by

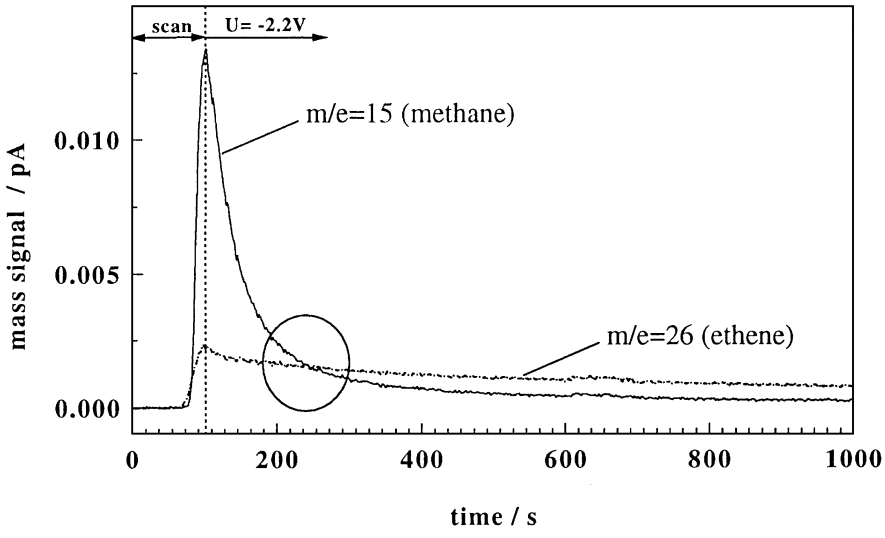

FIG. 5. Mass signals of methane and ethene versus time in 0.5 *M* $CsHCO_3/CO_2$-saturated electrolyte. After about 230 s. The ethene signal exceeds the mass signal of methane (circle). Profiles of the potential scan are as indicated in the legend to Fig. 3.

subtracting the baseline and normalized to the hydrogen mass signal as explained above.

Methane. It is seen that both rising and maximum peak signals of methane depend on the nature of the alkali ion: The highest and steepest signal is obtained with Rb^+ ($r =$ 152 pm), followed by the biggest investigated cation, Cs^+ ($r = 176$ pm) and K^+ ($r = 138$ pm). The methane signals for the smaller ions Na^+ ($r = 99$ pm) and Li^+ ($r = 59$ pm) are relatively low. Since the IR drop has been compensated, the resistance of the electrolyte cannot be the reason for different CO_2 reduction activity.

After passing the maximum value, the mass signals decay to a very low level. For all cations, except for Rb^+, the production rate at the end of the electrolysis is negligible compared to the peak maximum. The course of deactivation depends on the alkali ion: The larger ions (Rb^+ and Cs^+) cause a steep decay, whereas the slope of the smaller cations (K^+, Na^+, and Li^+) is rather smooth.

Ethene. Unlike the methane signal, different features can be observed for the production of ethene (Fig. 4b). The reduction activity for ethene production is negligible with small alkali ions Na^+ and Li^+. The ethene formation starts remarkably with K^+ and the highest production maximum is again obtained with Rb^+, followed by Cs^+. The deactivation process is qualitatively different. This is clearly evident from comparing the curves of cesium (Fig. 5): The deactivation process, which is different for methane and ethene formation, leads to a crossing of the curves of methane and ethene. After about 240 s the ethene mass signal is higher than that of methane. Apparently the adsorbing sites on the electrode surface are not the same for methane and ethene formation and different poisoning intermediates are formed with different affinities to these sites. An additional explanation can be due to a protonating step. Methane needs four of these reaction steps per C atom and can be more likely affected by a loss of reaction sites than ethene, which only needs two protons per carbon.

For the other ethene-forming cations Rb^+ and K^+ the observed deactivation rate for ethene is lower than for methane. However, with these cations the effect is smaller than with Cs^+. This experimental evidence shows that the adsorption of alkali cations plays a key role on the activity and selectivity of methane and ethene production.

Mass signal 31. Together with the formation of ethene, the $m/e = 31$ product was only significant in electrolytes containing K^+, Rb^+, or Cs^+. The mass signals are very small. A connection between $m/e = 31$ and a soluble poisoning compound with the same m/e, resulting from a mass fragment of a bigger molecule was rejected: The deactivation decay is very similar to that of ethene, probably their reaction paths are closely related. Ethene shows a low solubility in aqueous solutions and a high vapor pressure. In the experiment, when the cathode was renewed without a change of the electrolyte, the latter was bubbled with carbon dioxide. This procedure must have driven out volatile products but it was not observed that the electrolyte could be regenerated by long CO_2 purging.

For the comparison of adsorption processes and the influence of the electrolyte on the electrode activity, not only must the maximum activity and the deactivation be taken into account but also the overall amount of the compounds produced. With DEMS, this can easily be done by integrating the mass signals within the electroreduction time. Figure 6 shows the integrated mass signals of the methane, ethene, and $m/e = 31$ products over the electroreduction time of 1000 s.

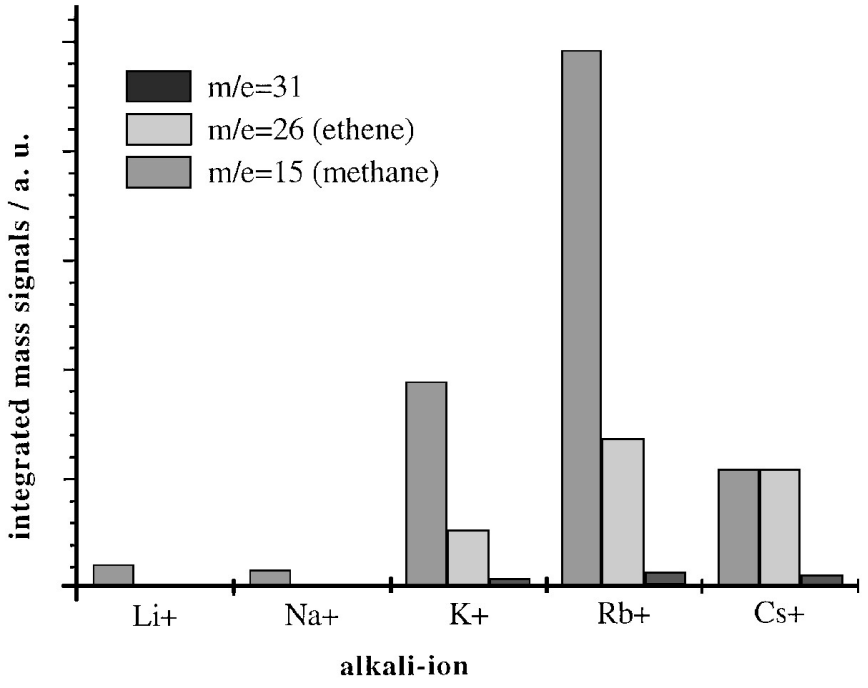

FIG. 6. Integrated standardized mass signals of methane, ethene, and $m/e = 31$ as a function of the electrolyte cation.

It should be noticed that the ionization and fragmentation probability are strongly dependent on the structure of the molecule. Therefore, similar mass signals do not necessarily mean similar production rates!

Figure 6 and Figs. 4a–4c show that smaller alkali cations such as Li^+ and Na^+ not only lead to a low activity maximum but also cause a small mass production over the integrated time. The maximal productivity is shown by Rb^+ regarding all three measured products. The following is K^+ for methane formation and Cs^+ for ethene and $m/e = 31$. These results demonstrate a qualitative difference to other measurements (16) that show an increasing overall methane production and decreasing overall ethene production with the size of the alkali ion. The reason for this might be the nondifferential analysis employed that included a longer duration of electrolysis. (60 min vs 16 min in our measurements). However, due to extremely low methane and ethene production rates at the end of our measurements such a drastic change in the results is unlikely.

Unfortunately it is not possible to deduce the total amount of reduced carbon dioxide from these integrated mass signals. Additionally, for this conclusion the oxidation number of the carbon atoms, the unknown substance $m/e = 31$ included, would have to be taken into account.

Summing up the effect of the cation, one can generally say that higher alkali ion radii cause a higher activity of CO_2 reduction. This can be connected to the lowering of the work function of the substrate by adsorption of alkali metals: The lower the ionization potential of the alkali metal, the larger the work function change (20). This might affect electron transfer and thus the activity of a catalytic system.

However, this does not explain the dependency of the product distribution on the alkali cation. Apparently, there must be different kinds of adsorption sites or geometries on the electrode surface which lead to different products. Depending on the electrolyte cation, some sites are preferred while others are not. Factors for this influence might be size, electronegativity as well as electron structure of the alkali ion.

Impedance measurements. Apparently the adsorption and charge transfer effects in the Helmholtz double-layer play an important role in the efficiency of carbon dioxide reduction. These effects cannot be investigated using only cyclovoltammetry and DEMS. Impedance measurements are very sensitive to surface reactions such as adsorption, desorption, or surface oxide removal. To get a better insight into the adsorption steps during the carbon dioxide reduction, the impedance technique was applied. In-phase (conductance) and quadrature component (capacity) of the impedance were recorded at 1 kHz (Figs. 7a and 7b).

The capacity and conductance curves were recorded starting at 0 V. A characteristic increase of both components at the beginning of the first scan could be observed with all investigated electrolytes. In the potential scan (0 to -1.7 V), one observes a similar feature of the in-phase and quadrature component, regarding the positions in potential

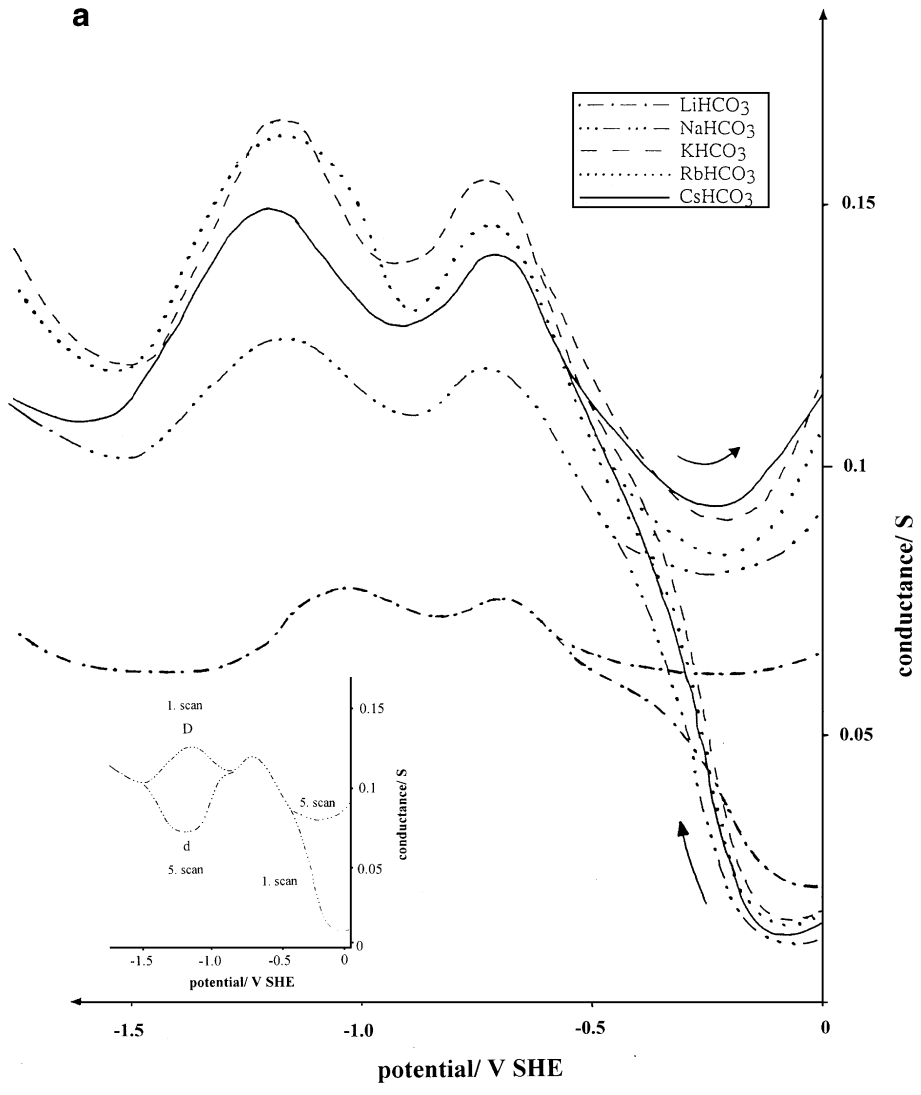

FIG. 7. (a) In-phase component (conductance) and (b) quadrature (capacity) of a copper electrode plotted versus the cell potential ($v = 5$ mV/s) in different hydrogencarbonate electrolytes. (Inset) The conductance before and after deactivation of the copper electrode.

of maxima and minima, which are mostly independent of the nature of the electrolyte cations. They only differ in their relative magnitudes. The rising part of each curve at the start of the measurement can be due to an activation (oxide removal) of the electrode surface.

The extrema of the in-phase and capacity plots reflect the copper surface state A change in the adsorbate structure influences both the capacity of the Helmholtz double layer and the AC conductivity. The lack of influence of the electrolyte cation on the extrema of the impedance components show that the adsorption process is the same for all alkali ions investigated and that there is no variation in the reaction path. But, if the electrolyte cation does not change the reaction path it may selectively favor the reaction rate of the seperate sideways, e.g., by changing adsorption energies of the intermediates.

The relative magnitude difference in the ordinate can be explained by the ohmic resistance of the electrolyte solutions which were 41.7 Ω (Li^+), 32.8 Ω (Na^+), 24.3 Ω (K^+), 24.0 Ω (Rb^+), 30.8 Ω (Cs^+), for 0.5 m HCO_3^- solutions (electrode distance 1 cm).

Performing several potential scans, another slower effect can be observed: After several cycles the maximum *D* in the conductance changes to a minimum *d* at the same potential (see inset Fig. 7a). This observation could be made on all investigated electrolytes. It coincides with the poisoning process of the copper electrode and can be interpreted as an irreversible formation of adsorbate which lowers the electron transfer in the double layer and thus leads to a decrease of the conductance.

So with impedance measurements the following observations could be made:

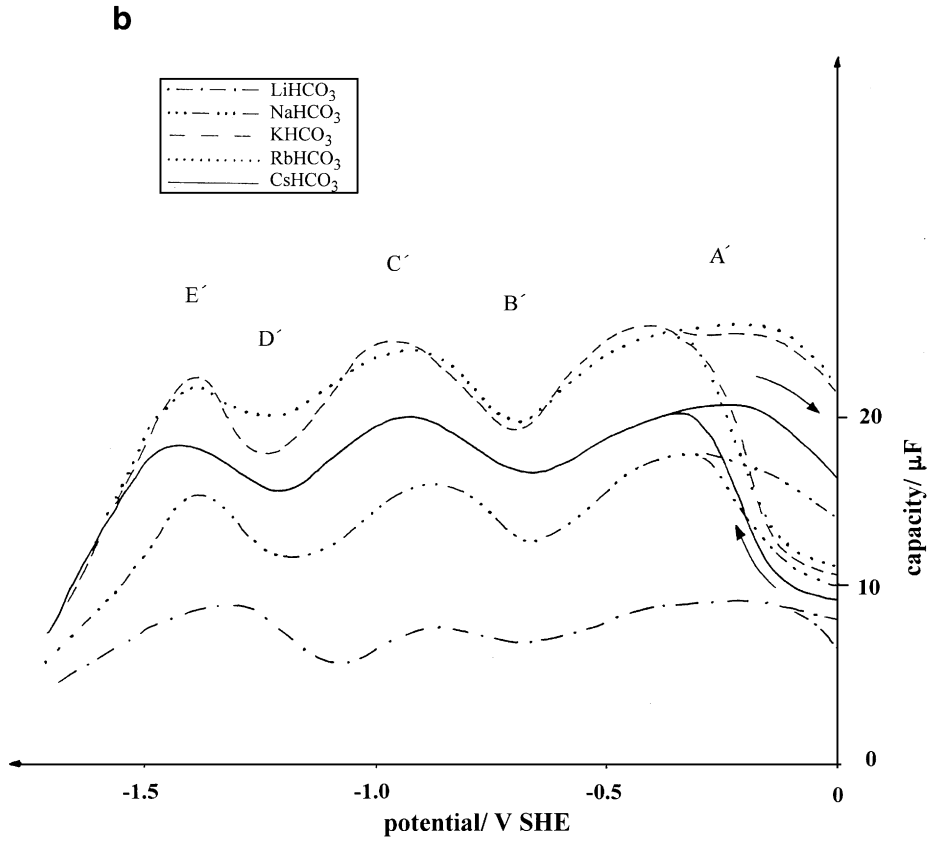

FIG. 7—*Continued*

There is an activation phase at the beginning of the first potential scan of a new electrode which is probably due to the reduction of a surface oxide layer.

Alkali ions in the electrolyte do not alter the reduction mechanism.

An irreversible adsorption happens in a potential area of −0.8 to −1.5 V and can be connected to the deactivation of the electrode.

Reaction Path

The mechanism of the CO_2 reduction is not yet established. The reaction step via a copper carbene was proposed by several groups (8, 23),

$$CO_2 \rightarrow\rightarrow\rightarrow CO^-_{2ads} \rightarrow\rightarrow\rightarrow Cu{=}CH_2 \rightarrow\rightarrow\rightarrow CH_4, C_2H_4, \quad [7]$$

in which the CO_2 molecule is adsorbed on the electrode surface by a nucleophilic attack on the partially positive C atom. This so-adsorbed molecular ion becomes further reduced and protonated in several reduction steps to form a carbene-like compound where the *d*-orbitals of the copper surface form a bond with two *p*-orbitals of each carbon atom. This carbene either gets further protonated to form a methane molecule or recombines with another carbene to ethene.

The potential scans under pulsed conditions as well as the different deactivation courses of methane and ethene production show that the reaction steps before as well as after the copper carbene suffer from poisoning effects. The occurrence of a black adsorbate suggests the presence of a graphite-like adsorbate, thus with an oxidation number between carbon dioxide and the carbene species.

Measurements in this work show that anodic pulses affect the production of methane and ethene in the same way. Presumably, the oxidative removal of the poisoning intermediates happens on the main branch before the reduction path splits into the sideways of methane and ethene formation. This means that electro-oxidation partially removes intermediates that are generated before the formation of the carbene species.

The copper carbene is the last "known" species that methane and ethene have in common (8, 23). The different deactivation course of methane and ethene and its dependence on the nature of the alkali cation shown in Figs. 4a–4c (the most striking contrast shows Cs^+, Fig. 5) points out that the influence of the electrolyte cations takes place after the formation of the carbene. Apparently the reduction

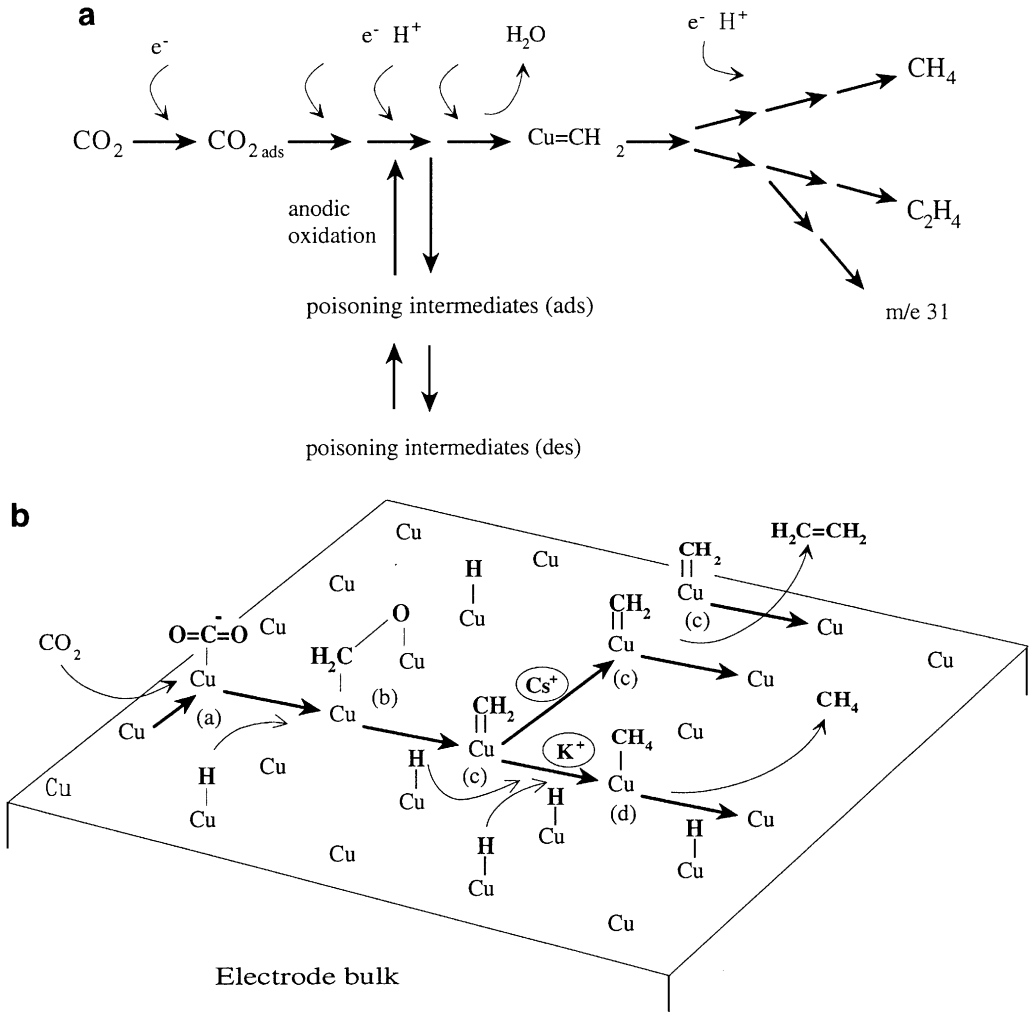

FIG. 8. Reaction pathway scheme of the electrochemical CO_2 reduction at copper.

as well as protonation steps and the recombination happen under different conditions and are influenced differently by the presence and adsorption of alkali ions. While K^+ and Rb^+ cause the same ratio methane/ethene of 3.7 and 3.8, respectively (values are taken from the integrated signal, Fig. 6), this ratio and the influence on the reaction path changes drastically when Cs^+ is used as cation (ratio 1.0). On the other hand, the influence does not only happen via the deactivation processes, otherwise the maximum production activities would be similar (see Figs. 4a and 4b).

Due to the similar course of the deactivation processes as well as the similar influence of the electrolyte cation of ethene and $m/e = 31$ it can be assumed that both molecules have a common reaction path (Fig. 8a). On the other hand, for combinatoric reasons it is not possible to construct a molecule fragment of $m/e = 31$ out of the atoms carbon, oxygen, and hydrogen that does not contain oxygen. Therefore, it can be concluded that a recombination process leads to a binding between the carbene species (c) (Fig. 8b) and the oxygen connected to copper of species (b). This recombination is favored by the bigger alkali cations K^+, Rb^+, and Cs^+ and suppressed by the smaller Na^+ and Li^+.

CONCLUSION

Deactivation measurements and investigations of the influence of the electrolyte cation give information about the reaction pathway and thus about the mechanism of the electrochemical reduction of carbon dioxide at copper electrodes. In the proposed reaction pathway (Figs. 8a and 8b) it can be seen that the results obtained in this work split mainly into two parts of the reaction path:

—The principal poisoning processes occur in the main branch of the path and this effect can be reduced by anodic oxidation.

—Adspecies such as alkali ions influence the CO_2 reduction activity of the cathode as well as the product

distribution. This effect takes place after the main reaction path has split up into several side reactions.

Regarding the deactivation of the electrode it should be noted that in subsequent investigations not only solid adsorbates should be observed but also the aging electroyte itself must be considered as a source of poisoning intermediates.

REFERENCES

1. Sammells, A. F., and Cook, R. L., *in* "Electrochemical and Electrocatalytic Reactions of Carbon Dioxide" (B. P. Sullivan, Ed.), p. 217. Elsevier, Amsterdam, 1993.
2. Ayers, W. M., *Spec. Publ. Roy. Soc. Chem*. **153**, 365 (1994).
3. Thampi, K. R., McEvoy, A. J., and Grätzel, M., *Spec. Publ. Roy. Soc. Chem*. **153**, 375 (1994).
4. Hori, Y., Kikuchi, K., and Suzuki, S., *Chem. Lett.* 1695 (1985).
5. Hori, Y., *et al*., *Chem. Lett.* 897 (1986).
6. Bittins-Cattaneo, B., *et al*., *in* "Electroanalytical Chemistry" (A. J. Bard, Ed.), Vol. 17, p. 1057. Dekker, New York/Basel/Hong Kong, 1991.
7. Bogdanoff, P., and Alonso-Vante, N., *Ber. Bunsenges. Phys. Chem*. **97**, 940 (1993).
8. Wasmus, S., Cattaneo, E., and Vielstich, W., *Electrochim. Acta* **35**, 771 (1990).
9. Bogdanoff, P., *et al*., manuscript in preparation.
10. Bogdanoff, P., and Alonso-Vante, N., *J. Electroanal. Chem*. **379**, 415 (1994).
11. Colell, H., and Alonso-Vante, N., manuscript in preparation.
12. DeWulf, D. W., Jin, T., and Bard, A. J., *J. Electrochem. Soc.* **136**, 1686 (1989).
13. Cook, R. L., MacDuff, R. C., and Samells, A. F., *J. Electrochem. Soc.* **134**, 1873 (1987).
14. Shiratsuchi, R., Aikoh, Y., and Nogami, G., *J. Electrochem. Soc.* **140**, 3479 (1993).
15. Jermann, B., and Augustynski, J., *Electrochim. Acta* **39**, 1891 (1994).
16. Kyriacou, G. Z., and Anagnostopoulos, A. K., *J. Appl. Electrochem*. **23**, 483 (1993).
17. Hori, Y., *et al*., "47th Annual meeting of ISE 1996." Veszprém, Hungary, in preparation.
18. Ikeda, S., *et al., Denki-Kagaku* **63**, 303 (1995).
19. Bonzel, H. P., and Krebs, H. J., *Surf. Sci.* **117**, 639 (1982).
20. Bonzel, H. P., *Surf. Sci. Rep.* **8**, 43 (1987).
21. Ertl, G., *Catal. Rev.-Sci. Eng.* **21**, 201 (1980).
22. Solymosi, F., *J. Mol. Catal.* **65**, 337 (1991).
23. Aurian-Blajeni, B., Halmann, M., and Manassen, J., *Solar Energy Mat.* **8**, 425 (1983).